ACS Photonics

Article

pubs.acs.org/journal/apchd5

Tunable Focusing in Natural Hyperbolic Magnetic Media

Rair Macêdo,*,† Thomas Dumelow,‡ and Robert L. Stamps†

†SUPA School of Physics and Astronomy, University of Glasgow, Glasgow G12 8QQ, United Kingdom

‡Departamento de Física, Universidade do Estado do Rio Grande do Norte, Costa e Silva, 59625-620 Mossoró, RN, Brazil

ABSTRACT: While optical effects such as negative refraction and imaging obtained from slab lenses with plane parallel sides are widely studied using metamaterials, it is less well known that these effects can occur naturally in certain materials. We discuss a class of natural hyperbolic materials that not only display similar effects but also allow one to modify the focal length of a slab lens with an externally applied magnetic field. This is possible because antiferromagnets are gyrotropic and support magnetic polaritons whose frequencies are sensitive to magnetic fields. In addition, a rich caustic structure emerges at low temperatures, when damping should be small. These materials also produce slab focusing at higher temperatures, although the caustic structure disappears.

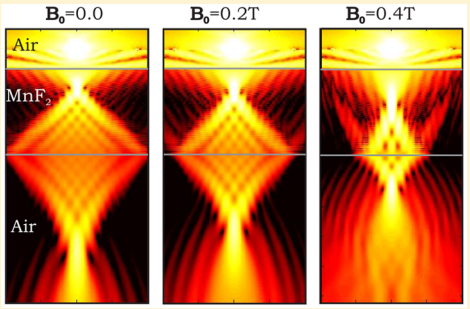

KEYWORDS: *negative refraction, lenses, magnon-polariton, antiferromagnets, THz*

The recent emergence of metamaterials has led to new optical devices.[1−3] For one intriguing class of materials, it is possible to focus light using lenses without physical curvature.[4] These lenses are just simple planar slabs with parallel sides. This concept was proposed long ago by Veselago and is based on the principle of negative refraction.[5] However, negative index materials exhibiting negative permittivity (ε) and permeability (μ) were only demonstrated experimentally over three decades after Veselago's proposition,[6] shortly after Pendry's seminal paper that showed how slabs of such materials could, in principle, act as perfect lenses, overcoming the diffraction limit that restricts image resolution in conventional lenses.[4]

Despite the early concentration on negative index materials with $\varepsilon < 0$ and $\mu < 0$, there have been several types of media proposed to obtain focusing in flat lenses. Of particular note are so-called hyperbolic media, which have rapidly gained attention for all-angle negative refraction with low loss.[7] These differ from negative index media in that the medium is typically nonmagnetic with $\mu = 1$, but the permittivity tensor is indefinite; that is, it has components with opposing signs along the principal axes. They are said to have hyperbolic dispersion due to the unusual relationship between the wavevector components resulting from indefinite permittivity. Although hyperbolic media are most often discussed in the context of artificial (metamaterial) structures,[8,9] hyperbolic behavior has been shown to exist for a number of natural single-phase crystals,[10,11] including quartz,[12] triglycine sulfate,[13] graphite,[14] or graphite-like materials such as magnesium diboride (MgB_2)[10] and tetradymites.[15] Even though natural hyperbolic materials are known to have the advantage of low losses, they have not yet been analyzed to the extent of artificial metamaterial structures. One of the reasons for this is that in artificial structures the components of the permittivity can normally be modified by varying the structural parameters.[16] In addition, these parameters can also be affected by external electric fields in some artificial structures,[17] which makes such structures of particular interest because of the possibility of controlling details of the optical properties. This is not possible in natural dielectric crystals, however.

There is, nevertheless, a class of natural materials that can be used to achieve tunable effects. The materials are magnetic crystals, which are not often associated with hyperbolic behavior. Here we propose tunable slab lensing in natural magnetic media using an externally applied magnetic field. Rather than the indefinite permittivity traditionally used to obtain hyperbolic dispersion, we make use of indefinite permeability in antiferromagnetic crystals; that is, not all the principal components of the $\vec{\mu}(\omega)$ tensors have the same sign. This phenomenon is present near the magnon-polariton resonances, where there are poles in selected components of the permeability, with negative values close to these poles. These poles can be shifted in frequency using applied magnetic fields. Because of this, at a given frequency, an external magnetic field $\mathbf{B_0}$ applied to an antiferromagnetic slab lens will shift the position of the image. We demonstrate this feature by calculating the focusing properties of THz radiation propagating through manganese fluoride (MnF_2), a reasonably well studied antiferromagnet.[18−21] We show also how interference associated with the refraction from a point source leads to caustic curves inside and outside the slab lens and examine the effect of temperature-dependent damping on these caustics.

We begin by noting some relevant electromagnetic properties of antiferromagnets. These materials are characterized by zero net magnetization except in the presence of an applied magnetic field. Although an average magnetization can be induced with a sufficiently large magnetic field, antiferromag-

Received: May 9, 2016
Published: August 16, 2016

DOI: 10.1021/acsphotonics.6b00321
ACS Photonics 2016, 3, 1670−1677

nets are not paramagnetic until above the so-called Néel temperature, T_N. Most recently, their static magnetic properties have been utilized as essential components in spintronic devices,[22,23] but they have long been understood to exhibit curious and potentially useful optical properties, such as nonreciprocal reflection.[24]

Such optical properties can be understood in terms of the permeability's dependence on frequency. Simple antiferromagnets have a magnetic unit cell with at least two distinct magnetic sublattices that are, in general, aligned antiparallel along the crystal's so-called easy axis when there are no external magnetic fields present. A dynamic response to time-varying magnetic fields appears as precessional motion of the magnetic sublattices, as depicted in the inset in Figure 1a, which shows

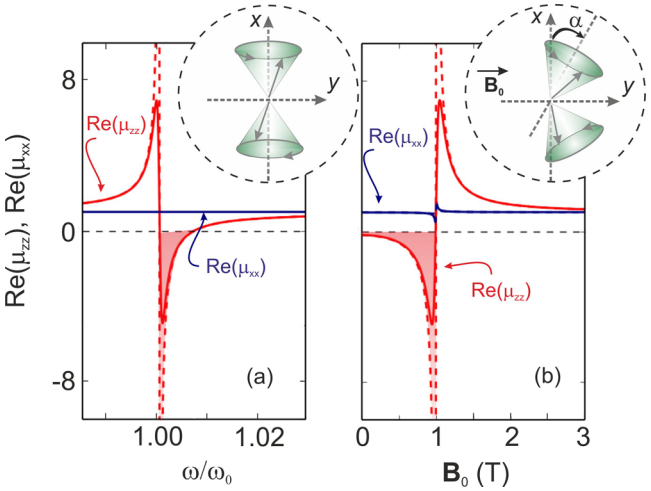

Figure 1. MnF_2 permeability: Real parts of the principal components of the permeability μ_{xx} and μ_{zz} (a) for $B_0 = 0$ and (b) as a function of applied magnetic field $\mathbf{B_0}$ at a frequency $\omega/\omega_0 = 1.005$. Dashed lines: $T = 0.06T_N$ (4.2 K). Solid lines: $T = 0.42T_N$ (28 K).

spins precessing in opposite directions. At low temperatures the dissipation of precession, and consequent resonance line widths, decreases strongly by suppressing scattering from lattice fluctuations. The amplitude of precession peaks at a resonant frequency ω_0 depends on the interactions responsible for the antiferromagnetic order and the magnetic anisotropy of the crystal.[25,26]

The resonances determine poles in the gyrotropic magnetic permeability tensor $\vec{\mu}(\omega)$,[27] represented as

$$\vec{\mu}(\omega) = \begin{pmatrix} \mu_{xx} & 0 & \mu_{xz} \\ 0 & \mu_{yy} & 0 \\ -\mu_{xz} & 0 & \mu_{zz} \end{pmatrix} \quad (1)$$

In zero applied magnetic field $\mathbf{B_0}$, the sublattices are perfectly aligned antiparallel to one another. Denoting these orientations as $+x$ and $-x$, the precession—and corresponding dynamic response—is in the transverse z and y directions. This means that μ_{xx}, which is shown in Figure 1a as a solid blue line, is unity at all frequencies, and the off-diagonal components μ_{xz} of eq 1 are always zero.

A strong magnon-polariton resonance occurs at $\omega/\omega_0 = 1.00$ and appears in the transverse components governed by μ_{zz} ($\mu_{zz} = \mu_{yy}$) shown as a red line in Figure 1a, being negative from $\omega/\omega_0 = 1.00$ to approximately 1.007 (shaded red region). The crystal is thus uniaxial along x, which serves as the optic axis.[28] Therefore, within the frequency range of interest, the permeability component along the optic axis is positive (=1), while that perpendicular to it is negative.

This behavior can be taken as the magnetic analogue of that of certain uniaxial nonmagnetic crystals close to the relevant phonon polariton resonances. Under the right conditions the effective permittivity tensor can have a positive component along the optic axis and a negative component perpendicular to it, in the same way as the antiferromagnet permeability tensor described here. Media displaying this type of anisotropy are frequently referred to as type II hyperbolic media.[11]

Distinct from nonmagnetic crystals, the hyperbolic behavior in magnetic media can be controlled with a magnetic field, which affects the magnon-polariton resonance frequency. If a magnetic field $\mathbf{B_0}$ is applied perpendicular to the zero field sublattice directions, the sublattice magnetizations will cant in order to align to the magnetic field direction. This canting is sketched in the inset of Figure 1b. In this case the precession has components along all coordinate axes, and all components of eq 1 display resonance poles. The main effect of $\mathbf{B_0}$ is simply to shift the resonances ω_0 to higher frequencies, however. Therefore, the resonance and its features, such as the condition to obtain negative refraction $\mu_{xx} > 0$ and $\mu_{zz} < 0$, are also tuned to different frequencies.[29] The red line in Figure 1b shows how, at a chosen frequency ($\omega/\omega_0 = 1.005$), μ_{zz} varies with an externally applied field, being negative over a wide range of field magnitudes (red shaded region).

The dynamic response of antiferromagnets to optical waves is determined by competition between components of the permeability tensor. Having now discussed the nature of resonances and general structure of the tensor, we now turn to the electromagnetic problem.

RESULTS

One finds that near resonance poles of the permeability it is possible to have conditions for negative refraction due to opposing signs on the elements of the permeability tensor. The corresponding features for slab transmission are now discussed.

Hyperbolic Dispersion and Negative Refraction. Hyperbolic media derive their name from the topology of their isofrequency curves, which are calculated from the dispersion relation between the frequency ω and the wave vector $\mathbf{k}$. In a vacuum, we have the linear relation

$$k_x^2 + k_{z1}^2 = \frac{\omega^2}{c^2} \quad (2)$$

In the geometry shown in Figure 2, we assume that the incident radiation, from a vacuum, is transverse electric (TE) polarized ($\mathbf{E}$ along y) with $k_y = 0$. The zero field optic axis is thus parallel to the surface of the crystal, within the plane of incidence (although, in the case of nonzero $\mathbf{B_0}$, this does not represent an exact description due to the loss of uniaxial symmetry). At frequency ω, the in-plane wave vector in the incident medium (vacuum) is given by $k_x = (\omega/c)\sin\theta_1$, where θ_1 is the incident angle.

Within the antiferromagnet, however, the permeability is a tensor $\vec{\mu}(\omega)$ with frequency-dependent components in the form shown by eq 1. In this case, waves with transverse electric polarization have a behavior described by a dispersion relation in the form

DOI: 10.1021/acsphotonics.6b00321
ACS Photonics 2016, 3, 1670−1677

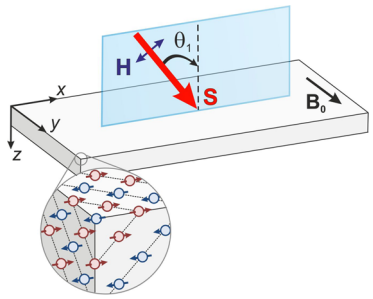

Figure 2. Geometry considered in this work: The sublattice magnetization and anisotropy fields are parallel to the surface and directed along the $+x$ and $-x$ axes. The inset shows the spin antiparallel arrangement in an antiferromagnetic slab.

$$k_{z2}^{2}\mu_{zz} + k_{x}^{2}\mu_{xx} = \frac{\omega^{2}}{c^{2}}\varepsilon(\mu_{xx}\mu_{zz} + \mu_{xz}^{2}) \tag{3}$$

Examples of isofrequency curves, which relate the principal components of the wavevector at a given frequency, are shown in Figure 3 for different values of externally applied field. In air

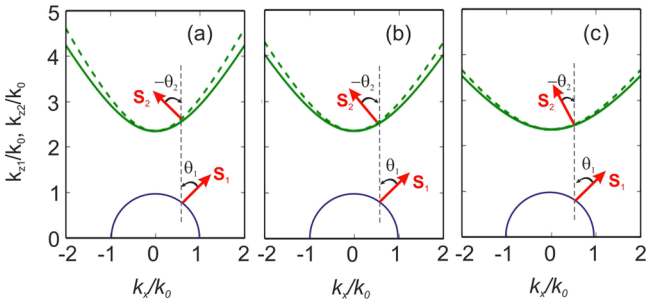

Figure 3. Isofrequency curves: Real parts of the wave-vector component k_{1z} (blue lines) and k_{2z} (green lines) as a function of k_x (expressed in units of k_0), for transmission in a MnF_2 crystal having its extraordinary axis directed along x, in s-polarization at a frequency $\omega/\omega_0 = 1.005$. (a) $B_0 = 0.0$, (b) $B_0 = 0.2$ T, and (c) $B_0 = 0.4$ T. Dashed lines: $T = 0.06T_N$ (4.2 K). Solid lines: $T = 0.42T_N$ (28 K).

(curves shown in blue) the linear dispersion and isotropic behavior of propagating waves imply a circular isofrequency curve given by eq 2. The circular isofrequency curve of air distorts to an ellipse for an anisotropic medium with positive ε and μ components. However, when we have extreme anisotropy, as occurs in MnF_2 close to the magnon-polarition resonance, such that $\mu_{xx}\mu_{zz} < 0$, the isofrequency curve opens into a hyperbola (shown as green lines in Figure 3).

The group velocity and hence the Poynting vector are perpendicular to the constant ω plots and are shown in Figure 3 as red arrows. Therefore, the x component of the Poynting vector ($\mathbf{S}_2$) inside the antiferromagnet is always in the opposite direction to that of the incident beam ($\mathbf{S}_1$).

When a small external field $\mathbf{B}_0$ is applied, the isofrequency curve becomes flatter than the equivalent zero field curve, as shown in Figure 3b and c. This is due to changes in the permeability tensor component μ_{zz}, which, for fields less than 1 T, is negative and field dependent, in line with Figure 1b.

In Figure 4 we show how the angle of refraction θ_2 can be tuned using an external magnetic field due to its effect on the permeability tensor components. This can be seen from the energy flow, which is usefully expressed as the time-averaged Poynting vector $\langle \mathbf{S}_2 \rangle = (1/2)\mathrm{Re}(\mathbf{E} \times \mathbf{H}^*)$. We calculate refraction of a beam of finite width, with a Gaussian profile in x and z, passing through a MnF_2 crystal 10λ thick, where λ is the free-space wavelength. The angle of incidence is set to 45°, and the Gaussian beam is focused at the slab surface. For $B_0 = 0.0$ at $\omega/\omega_0 = 1.005$, negative refraction is seen as a displacement of the transmitted beam in the negative x direction (see Figure 4a). Note that the behavior for all $\mathbf{B}_0$ values in the chosen range is qualitatively similar. However, the angle of refraction becomes smaller as the field is increased, as predicted from Figure 3. The black arrows showing the direction of the power flow were calculated using the relation given by eq 14.

Caustics and Field-Tunable Focusing. We have seen how all angle negative refraction can be achieved inside an antiferromagnet due to its hyperbolic dispersion as shown in Figure 3. As a result, if a point source is placed close to an antiferromagnetic flat lens with parallel sides, it is possible to obtain focusing within the lens, with a second focus on the other side of it. Thus, an object placed on one side of the lens can form an image on the other side in a manner similar to that described by Pendry[4] for media with $\varepsilon < 0$ and $\mu < 0$. In the paraxial limit, i.e., small angles of incidence, focusing, i.e., image formation, effectively occurs at a single focal point, as seen from Figure 5a. Therefore, the lens equation for this type of system simply relates the image distance d_3 to the object distance d_1, the thickness d_2 of the lens, and its effective index of refraction n_{eff} for use in Snell's law. It can be obtained by either geometric optics[13] or wave optics[30] and is given by

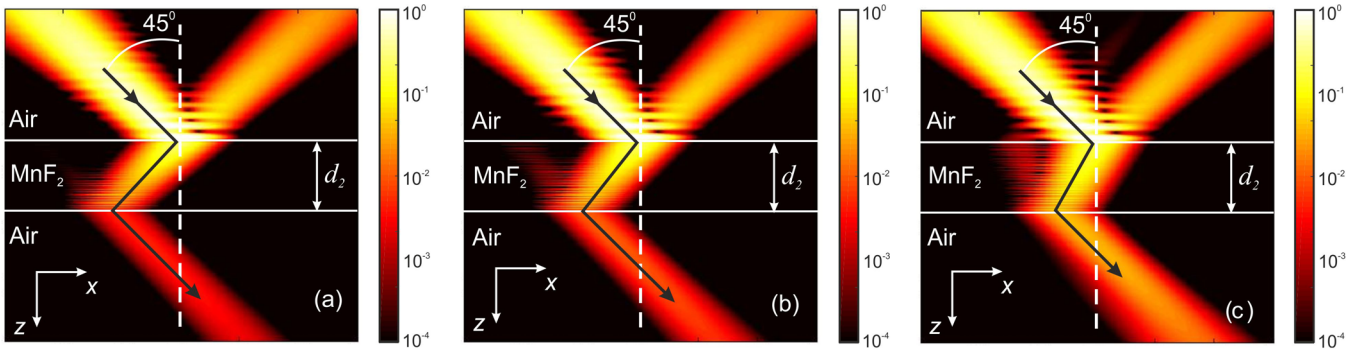

Figure 4. Negative refraction: (a) Intensity profile (time-averaged power density) of a Gaussian beam obliquely incident at an angle of incidence $\theta_1 = 45°$, passing through a MnF_2 slab of thickness $d_2 \approx 1.0$ cm at frequency $\omega/\omega_0 = 1.005$ where $\omega_0 = 8.67$ cm^{-1} ($T = 0.06T_N$ (4.2 K)). (a) $B_0 = 0.0$, (b) $B_0 = 0.2$ T, and (c) $B_0 = 0.4$ T. The intensity scale is in arbitrary units.

DOI: 10.1021/acsphotonics.6b00321
ACS Photonics 2016, 3, 1670−1677

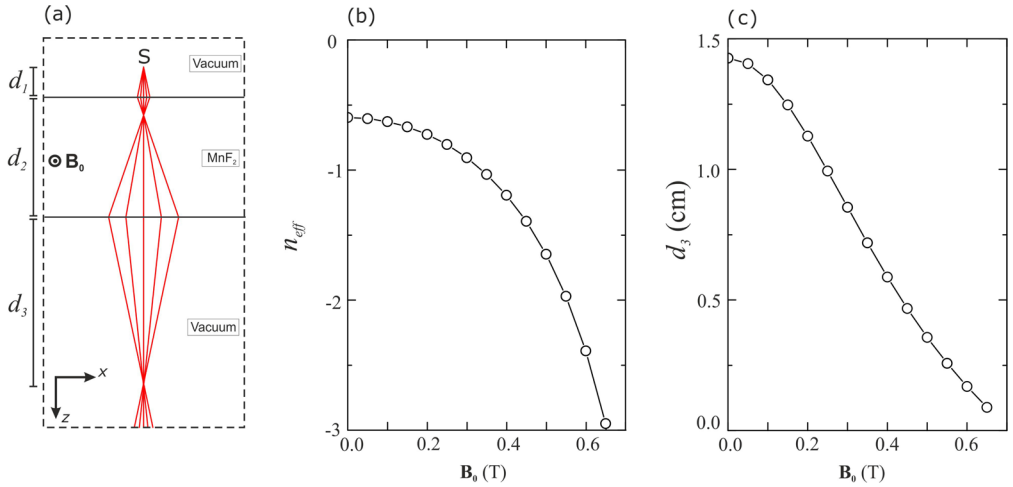

Figure 5. Tunable image formation achieved with an applied magnetic field: (a) Schematic of focusing due to a source S placed above a MnF_2 slab in the absence of an external field ($B_0 = 0.0$). The incident angle is restricted to the range $-10°$ to $+10°$. The distance d_1 is equal to 0.25 cm, and the slab thickness d_2 is equal to 1.0 cm. The extraordinary axis is directed along x and incident radiation at $\omega/\omega_0 = 1.005$. Effect of an externally applied magnetic field $\mathbf{B_0}$ is shown for (b) the effective index of refraction n_{eff} and (c) the image distance d_3.

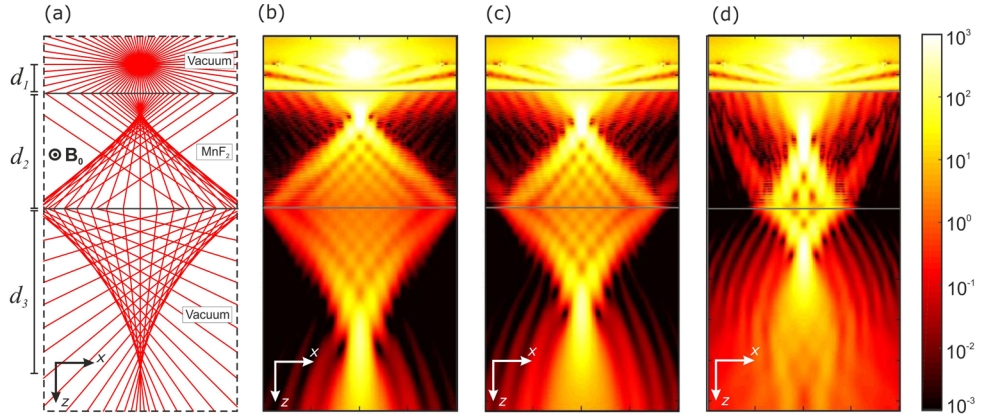

Figure 6. Image formation and caustics: s-polarization image formation at $T = 0.06T_N$ (4.2 K) due to a line source placed above a MnF_2 slab. The slab thickness d_2 is $20\lambda'$ (≈1.0 cm), where λ' represents the wavelength within the antiferromagnet at normal incidence (about half the free-space wavelength). The distance d_1 is equal to $d_2/4$ (≈0.25 cm). The extraordinary axis is directed along x, and the frequency of the incident radiation is $\omega/\omega_0 = 1.005$. (a) Schematic showing the path of multiple rays passing through a MnF_2 slab for $B_0 = 0.0$. (b) Power flow intensity for the setup shown in (a). Effect of a magnetic field on the intensity profile for (c) $B_0 = 0.2$ T and (d) $B_0 = 0.4$ T. The intensity scale is in arbitrary units.

$$d_1 + d_3 = -\frac{d_2}{n_{\text{eff}}} \tag{4}$$

where n_{eff} is given by

$$n_{\text{eff}} = \frac{\varepsilon^{1/2}\mu_{zz}}{\mu_{xx}^{1/2}}\left(1 + \frac{\mu_{xz}^{2}}{\mu_{xx}\mu_{zz}}\right)^{1/2} \tag{5}$$

The form of these equations is equivalent to those shown for lenses made of nonmagnetic hyperbolic media.[13] In the present case, n_{eff} is negative in the frequency regime where $\mu_{zz} > 0$ and u$\mu_{zz} < 0$. However, an exciting feature of magnetic crystals is the fact that n_{eff} strongly depends on μ_{zz}, whose value is highly reliant on external applied fields, as seen from Figure 1b. The effect of an externally applied field on the effective index of refraction can be seen in Figure 5b. One consequence of a nonzero field is that the image position can be tuned, as the angle of refraction depends on the effective index of refraction. The effects of a field $\mathbf{B_0}$ on the distance d_3 between the image and the lens is illustrated in Figure 5c, which shows d_3 decreasing as the strength of the field $\mathbf{B_0}$ increases. It is also worth mentioning another consequence of an externally applied field: the off-diagonal components in the permeability tensor become nonzero (i.e., gyromagnetic), and these off-diagonal components also affect n_{eff},[29] although in practice the effect is negligible.

Although the image formed by an antiferromagnetic lens is real, it is not perfect. In a hyperbolic medium the focusing of peripheral rays occurs at positions that cannot be described by the paraxial approximation. In order to illustrate this, we show, in Figure 6a, a ray diagram representing focusing over a wide range of incident angles. Marginal rays are focused after the paraxial focus within the slab and before the paraxial focus outside the slab. This leads to an envelope of interfering refracted rays, i.e., caustics.

In Figure 6b we show the behavior of the power flow, given by the time-average Poynting vector $\langle \mathbf{S}_2 \rangle$ of radiation emanating from the line source, directed along y, at a frequency $\omega/\omega_0 = 1.005$ and temperature $0.06T_N$, in the absence of an externally applied field. Due to high levels of transmission for all incident angles, intersecting rays produce a network of constructive and destructive interference within the caustic

DOI: 10.1021/acsphotonics.6b00321
ACS Photonics 2016, 3, 1670−1677

envelope, both inside and outside the slab. This is most visible when damping is extremely low (as would be expected at low temperatures for good crystals). Nevertheless, despite the complications of the caustics due to imperfect focusing at high angles, there is a high intensity sharp focus at the cusp. Figure 6c and d show how the image is moved closer to the lens by simply applying an external field, as predicted by Figure 5c.

As well as investigating image formation at $0.06T_N$, we have also considered higher temperatures; an example is shown for $0.42T_N$, leading to a significant increase in magnon damping within the antiferromagnet. The effect of this is to reduce transmission at higher angles, as shown in Figure 7, which

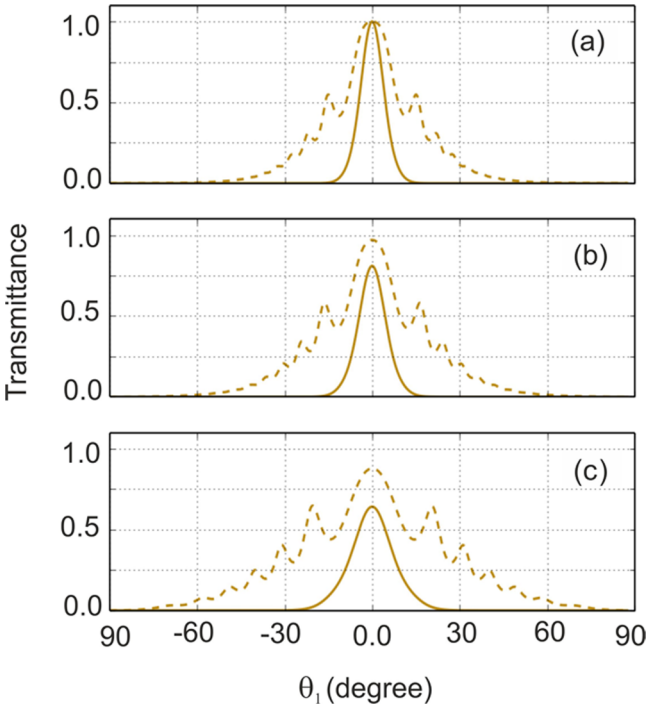

Figure 7. Transmission in MnF_2: Calculation of trasmittance as a function of incidence angle (θ_1) for an MnF_2 slab of thickness $d_2 = 20\lambda'$ (≈1.0 cm) whose easy axis lies along x. The incident radiation, at a frequency $\omega/\omega_0 = 1.005$, is s-polarized. (a) $B_0 = 0.0$, (b) $B_0 = 0.2$ T, and (c) $B_0 = 0.4$ T. Dashed lines: $T = 0.06T_N$ (4.2 K). Solid lines: $T = 0.42T_N$ (28 K).

compares the angular dependence of transmittance at the two temperatures. The figure shows that, at the higher temperature, efficient transmission occurs only within the range ±20°. This behavior can effect the properties of a lens made of an antiferromagnet, the result of which can be seen in the sketch in Figure 8a, which shows exclusively the focusing of small-angle incident rays, leading to paraxial-type behavior.

Since, at high angles of incidence, there is little propagation inside the slab, there is not much interference emanating from these rays with higher damping, and the envelope of refracted rays forming a well-defined caustics fold is lost, as seen from the power flow behavior shown in Figure 8b. However, the radiation focusing is still present as a strong cusp, and the tunable image position is also unaffected by the temperature change, although, due to the loss of high angular components, the effect of the field is less obvious, as seen in Figure 8c and d. Nevertheless, these components will be more prominent in the case of thinner slabs, leading to the restoration of much of the structure shown in Figure 6.

DISCUSSION

The network of intensities discussed above are examples of caustic curves analogous to those discussed in the classic works by Nye.[31] These caustics are a result of the nonperfect focusing due to hyperbolic behavior of antiferromagnets. The shape of these caustics can be modified by changing the magnitude of the external applied field $\mathbf{B_0}$. We believe that the method to obtain caustics that we have reported should be possible in any hyperbolic media given a damping low enough to enable transmission of all incident angles.

The key point here is that for hyperbolic magnetic media not only can a caustic structure be seen but focusing can also be achieved in a slab lens. Similar focusing has been reported in other natural hyperbolic media such as quartz crystals[12] and triglycine sulfate.[13] In both cases this occurs for p-polarized radiation with a distinct image position that varies with frequency, due to the way that phonons couple with the electric part of the electromagnetic radiation. However, natural magnetic media are field reliant, which allows tunable image formation at a single frequency without changing the crystal structure or the physical shape of the lens.

In this work, we have concentrated on using an external magnetic field to adjust the image position for a fixed source position. However, the external field is effectively tuning the overall object−image distance. Thus, one could, in principle, consider a slightly different configuration in which a detector (or detector array) was placed at the surface of the slab (or a fixed distance from it). Assuming that there is an illuminated object at a certain unknown distance from the other side of the slab, this distance could then be measured by scanning the applied magnetic field and determining the field at which the image became well focused on the detector. In this case, the lens would act as a type of depth probe, suitable for investigating objects embedded in a medium transparent to the relevant terahertz radiation. The slab (with detector) could be placed at the surface of the medium. The medium would then be irradiated with monochromatic terahertz radiation, which would be scattered from the embedded objects, in the presence of an applied field.

Although all our results are restricted to focusing in the far-field limit, we also expect that these intriguing findings will benefit near-field and subwavelength imaging. Normally, for free-space or isotropic media, k_z is real, but when k_x becomes large, k_z becomes imaginary; that is, the propagation of waves in the z direction is evanescent: it decays exponentially with z. However, in the case of indefinite permeability, k_z is real for all k_x values, even for very large ones. Therefore, what would normally be evanescent waves, now become propagating waves.[7,12] In this case, the emitted evanescent waves of a light source placed near a slab with arbitrarily large in-plane wave vectors can excite propagating modes in the slab, which will transfer the near-field information to the opposite interface of the slab, as shown experimentally in the analogous indefinite permittivity case based on the phonon polariton response in hexagonal boron nitride.[32] At the magnon resonance frequency itself, all components should transmit across within the slab with the same phase, and a faithful reproduction of subwavelength details of the object should be possible.[12] The use of an external field should allow some fine-tuning, as the resonance frequency can be shifted when applying such a field.

In this article we have considered only slab lenses made from MnF_2, a material that shows particularly low magnon damping

DOI: 10.1021/acsphotonics.6b00321
ACS Photonics 2016, 3, 1670−1677

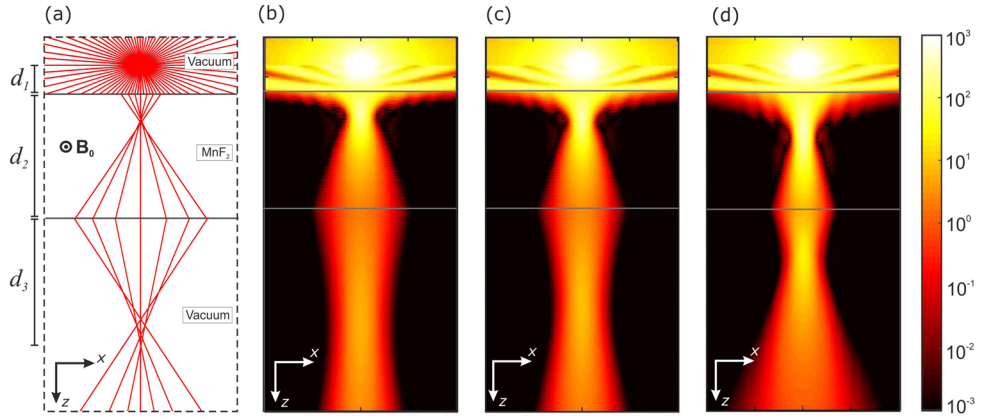

Figure 8. Tunable focusing: s-polarization image formation at $T = 0.42T_N$ (28 K) due to a line source placed above of a MnF_2 slab. The slab thickness d_2 is $20\lambda'$ (≈1.0 cm), and d_1 is equal to $d_2/4$ (≈0.25 cm). The extraordinary axis is directed along x and incident radiation at $\omega/\omega_0 = 1.005$. (a) Schematic showing the path of multiple rays passing through a MnF_2 slab for $B_0 = 0.0$. (b) Power flow intensity for the setup shown in (a). Effect of a magnetic field on the intensity profile for (c) $B_0 = 0.2$ T and (d) $B_0 = 0.4$ T. The intensity scale is in arbitrary units.

at low temperature. However, this material belongs to an important group of antiferromagnetic salts, such as iron fluoride (FeF_2) and cobalt fluoride (CoF_2), which should also display similar behavior at temperatures far enough below their Néel temperatures.[27] Antiferromagnets whose Néel temperatures fall above room temperature are hard to come by (although there are exceptions, such as nickel oxide, NiO), and, in addition, various dissipation mechanisms can severely limit THz frequency wave transmission at higher temperatures. For instance, recent experiments with NiO have reported $\Gamma/\omega_0 = 7 \times 10^{-2}$,[33] which is extremely high for efficient slab lenses. Nevertheless, alternative magnetic crystals, such as ferrites, display field-tunable hyperbolic dispersion, similar to that discussed here, associated with the ferromagnetic resonance.[34] Such materials may well be suitable for use as tunable slab lenses at room temperature in much the same way as shown here for MnF_2 at low temperature, although some fine structure associated with interferences may still not appear except at low temperatures.

Finally, we stress that the analysis and general principles presented in this article apply equally well to other types of hyperbolic media, both natural and artificial.

METHODS

Magnon-Polariton Resonances in Antiferromagnets. The spins in a simple antiferromagnet are aligned by exchange interactions so that they are spontaneously magnetized in opposite directions. As a result, the magnetic moment (M_S) will point predominantly parallel and antiparallel to a preferred axis (here defined as x) bound by anisotropic forces arising from dipole−dipole interactions and from field effects.[19] If an electromagnetic wave strikes the antiferromagnet surface, the magnetic field of the radiation ($\mathbf{H}$) interacts with the spins in the material, inducing precessional motion that should be resonant at the frequency

$$\omega_0 = \gamma(2B_AB_E + B_A{}^2)^{1/2} \tag{6}$$

B_A and B_E are effective fields representing the forces constraining the sublattice magnetizations to the preferred axis. B_A measures the anisotropy force and B_E the exchange force that is exerted on each ion by the ions forming the other sublattice.[18]

When there is no externally applied field, there is no interaction along x; therefore μ_{xx} does not differ from unity at any frequency, and the other tensor components are given by

$$\mu_{yy} = \mu_{zz} = 1 + \frac{2\mu_0\gamma^2M_SB_A}{\omega_r{}^2 - (\omega + i\Gamma)^2} \tag{7}$$

Resonance Tuning by Externally Applied Field B_0. If an external field is applied perpendicular to the spins' alignment direction (here taken as y), the spins cant at an angle α in the plane xy calculated in terms of B_A and B_E.[21] The angle α is then given by

$$\sin\alpha = \frac{B_0}{B_A + 2B_E} \tag{8}$$

One can show that the antiferromagnetic resonance frequency is now[21]

$$\omega_r = (\omega_0{}^2\cos^2\alpha + 2\gamma^2B_0B_E\sin\alpha)^{1/2} \tag{9}$$

When $\mathbf{B_0}$ is nonzero, the resonance frequency is now shifted to higher frequencies depending on the magnitude of the external field. Not only that, but the off-diagonal elements μ_{xz} and μ_{zx} are nonzero and μ_{xx} differs from unity close to the resonance frequency. It happens only due to the canting of the spins, which results in a small spin component along the applied field direction.[35]

In this case, the relevant components are[21]

$$\mu_{xx} = 1 + \frac{2\mu_0\gamma^2M_SB_0\sin\alpha}{\omega_0{}^2 - (\omega + i\Gamma)^2} \tag{10}$$

$$\mu_{zz} = 1 + \frac{2\mu_0\gamma^2M_S(B_0\sin\alpha + B_A\cos 2\alpha)}{\omega_0{}^2 - (\omega + i\Gamma)^2} \tag{11}$$

and

$$\mu_{xz} = -\mu_{xz} = -i\frac{2\mu_0\gamma^2M_S(\omega + i\Gamma)\sin\alpha}{\omega_0{}^2 - (\omega + i\Gamma)^2} \tag{12}$$

Angle and Effective Index of Refraction. In order to calculate the angle of refraction θ_2 within the antiferromagnetic slab, we look at the power flow $\mathbf{S}_2$. For waves with transverse electric polarization, the power flow can be represented as the

DOI: 10.1021/acsphotonics.6b00321
ACS Photonics 2016, 3, 1670−1677

time-averaged Poynting vector $\langle \mathbf{S}_2 \rangle = (1/2)\mathrm{Re}(\mathbf{E} \times \mathbf{H}^*)$. For the general case when an external field is applied, $\mathbf{B}_0 \neq 0$; this gives

$$\langle \mathbf{S}_2 \rangle = \frac{|E_y|^2}{2\omega\mu_0}\mathrm{Re}\left(\frac{k_x\mu_{xx} - k_{2z}\mu_{xz}}{\mu_{xx}\mu_{zz} + \mu_{xz}^{\ 2}}, 0, \frac{k_{2z}\mu_{zz} + k_x\mu_{xz}}{\mu_{xx}\mu_{zz} + \mu_{xz}^{\ 2}} \right) \tag{13}$$

Thus, the angle of refraction θ_2 is given by

$$\tan\theta_2 = \frac{\langle S_{2x} \rangle}{\langle S_{2z} \rangle} \tag{14}$$

In order to find the medium's index of refraction, it is useful to apply Snell's law, which, for refraction from vacuum into an isotropic medium, gives $\sin\theta_1/\sin\theta_2 = n$, where n is the refractive index of the medium. In determining the effective index n_{eff} for the antiferromagnet, we take the sines of the two angles in the small-angle limit ($k_x \ll \omega/c$). In the zero-damping case, for which $\mathrm{Re}(\mu_{xz}) = 0$, this gives

$$\sin\theta_1 = \frac{k_x c}{\omega} \tag{15}$$

$$\sin\theta_2 \approx \tan\theta_2 = \frac{k_x\mu_{xx}}{k_{z2}\mu_{zz}} \approx \frac{k_x\mu_{xx}c}{\omega\varepsilon^{1/2}(\mu_{xx}\mu_{zz} + \mu_{xz}^{\ 2})^{1/2}\mu_{zz}^{\ 1/2}} \tag{16}$$

Comparing these two results gives the effective index of refraction n_{eff} presented earlier as eq 5.

Parameters Used. The antiferromagnetic ordering of spins appears in MnF_2 at temperatures below its Neél temperature $T_N = 67$ K, with a zero-field resonance frequency ω_0 given by eq 6. In this work, we have used the field parameters reported by Remer et al.,[20] i.e., $B_A = 0.787$ T and $B_E = 55.0$ T, who also report $M_S = 6.0 \times 10^5$ A/m and $\varepsilon = 5.5$.

In order to analyze the effects of temperature on the focusing by an antiferromagnetic slab lens, we have considered two different temperatures: 4.2 K, which corresponds to $0.06T_N$, and 28 K, which corresponds to $0.42T_N$. Within the temperature range considered here, the variation in the resonance frequency ω_0 is fairly small. Therefore, for simplicity, we just model it as a change in the gyromagnetic ratio γ. Thus, at a temperature of $0.06T_N$, we have $\gamma/2\pi c = 0.928$ cm^{-1}/T, corresponding to a resonance frequency of $\omega_0/2\pi c = 8.67$ cm^{-1}, whereas at a temperature of $0.42T_N$ we have $\gamma/2\pi c = 0.877$ cm^{-1}/T, corresponding to a resonance frequency of $\omega_0/2\pi c = 8.19$ cm^{-1}. The corresponding damping parameters used here are[20] $\Gamma/\omega_0 = 8 \times 10^{-5}$ at $0.06T_N$ and $\Gamma/\omega_0 = 6.5 \times 10^{-4}$ at $0.42T_N$.

Intensity Profile Calculations. The intensity profiles shown in Figures 4, 6, and 8 were calculated using a plane wave spectrum model. In the case of Figure 4, in which a Gaussian beam is incident upon a magnetic hyperbolic crystal, this means that we take the incident beam to be a Fourier sum of plane waves, represented as

$$E_y = \int_{-\infty}^{\infty} \psi(k_x)\, \mathrm{e}^{\mathrm{i}(k_x x + k_{zi} z)}\, \mathrm{d}k_x \tag{17}$$

where $\psi(k_x)$ is the Gaussian spectrum, which carries the information on the shape of the beam centered at $x = 0$ and $z = 0$ and is given by[29,36,37]

$$\psi(k_x) = -\frac{g}{2\cos\theta_1\sqrt{\pi}}\exp\left[-\frac{g^2(k_x - k_0\sin\theta_1)^2}{4\cos^2\theta_1} \right] \tag{18}$$

Here $2g$ represents the beam width at its waist and θ_1 the incident angle of the central plane wave.

When traveling through a slab as proposed here, the fields have to be separated for each of the three distinct layers n and can be represented as

$$E_y = \int_{-\infty}^{\infty} [a_n(k_x)\, \mathrm{e}^{\mathrm{i}k_{zn}z} + b_n(k_x)\, e^{-\mathrm{i}k_{zn}z}]\, e^{\mathrm{i}k_x x}\, \mathrm{d}k_x \tag{19}$$

The coefficients a_n and b_n are for radiation propagating in the direction of increasing and decreasing z respectively. $n = 1$ represnts the incident layer, so $a_1 = y(kx)$. In addition, there is no propagation in the negative z direction in the final layer, so $b_3 = 0$. The other coefficients may be calculated using standard transfer matrix techniques in a manner similar to that described by Dumelow and Camley.[38]

In order to model focusing in an antiferromagnet as shown in Figure 6a and Figure 8a, a source radiating in all directions in the xz plane must be used. We consider an oscillating line of electric current I directed along the y axis placed at $x = 0$ and $z = 0$. The analysis is essentially the same as that used for the Gaussian beam as described previously, but with $\psi(k_x)$ now given by

$$\psi(k_x) = \frac{\omega\mu_0 I}{4\pi k_{1z}} \tag{20}$$

AUTHOR INFORMATION

Corresponding Author

*E-mail: Rair.Macedo@glasgow.ac.uk.

Notes

The authors declare no competing financial interest.

ACKNOWLEDGMENTS

The authors thank R. E. Camley and D. A. MacLaren for helpful discussions. This work was supported by EPSRC EP/M024423/1 and the Brazilian research agency CNPq.

REFERENCES

(1) Zheludev, N. I.; Kivshar, Y. S. From metamaterials to metadevices. *Nat. Mater.* **2012**, *11*, 917−924.
(2) Shalaev, V. M. Transforming light. *Science* **2008**, *322*, 384−386.
(3) Ou, J. Y.; Plum, E.; Jiang, L.; Zheludev, N. I. Reconfigurable photonic metamaterials. *Nano Lett.* **2011**, *11*, 2142−2144.
(4) Pendry, J. B. Negative refraction makes a perfect lens. *Phys. Rev. Lett.* **2000**, *85*, 3966−3969.
(5) Veselago, V. G. The electrodynamics of substances with simultaneously negative values of ε and μ. *Sov. Phys. Usp.* **1968**, *10*, 509−514.
(6) Shelby, R. A.; Smith, D. R.; Schultz, S. Experimental verification of a negative index of refraction. *Science* **2001**, *292*, 77−79.
(7) Poddubny, A.; Iorsh, I.; Belov, P.; Kivshar, Y. Hyperbolic metamaterials. *Nat. Photonics* **2013**, *7*, 948−957.
(8) Dong, J.-W.; Zheng, H. H.; Lai, Y.; Wang, H.-Z.; Chan, C. T. Metamaterial slab as a lens, a cloak, or an intermediate. *Phys. Rev. B: Condens. Matter Mater. Phys.* **2011**, *83*, 115124.
(9) Yao, J.; Tsai, K.-T.; Wang, Y.; Liu, Z.; Bartal, G.; Wang, Y.-L.; Zhang, X. Imaging visible light using anisotropic metamaterial slab lens. *Opt. Express* **2009**, *17*, 22380.
(10) Sun, J.; Litchinitser, N. M.; Zhou, J. Indefinite by nature: From ultraviolet to terahertz. *ACS Photonics* **2014**, *1*, 293−303.
(11) Korzeb, K.; Gajc, M.; Dorota, A. P. Compendium of natural hyperbolic materials. *Opt. Express* **2015**, *20*, 25406−25424.
(12) Estevâm da Silva, R.; Macêdo, R.; Dumelow, T.; da Costa, J. A. P.; Honorato, S. B.; Ayala, A. P. Far-infrared slab lensing and

DOI: 10.1021/acsphotonics.6b00321
ACS Photonics 2016, 3, 1670−1677

subwavelength imaging in crystal quartz. *Phys. Rev. B: Condens. Matter Mater. Phys.* **2012**, *86*, 155152.
(13) Dumelow, T.; da Costa, J. A. P.; Freire, V. N. Slab lenses from simple anisotropic media. *Phys. Rev. B: Condens. Matter Mater. Phys.* **2005**, *72*, 235115.
(14) Sun, J.; Zhou, J.; Li, B.; Kang, F. Indefinite permittivity and negative refraction in natural material: Graphite. *Appl. Phys. Lett.* **2011**, *98*, 101901.
(15) Esslinger, M.; Vogelgesang, R.; Talebi, N.; Khunsin, W.; Gehring, P.; de Zuani, S.; Gompf, B.; Kern, K. Tetradymites as natural hyperbolic materials for the near-infrared to visible. *ACS Photonics* **2014**, *1*, 1285−1289.
(16) Forouzmand, A.; Yakovlev, A. B. Tunable dual-band subwavelength imaging with a wire medium slab loaded with nanostructured graphene metasurfaces. *AIP Adv.* **2015**, *5*, 077108.
(17) Shi, L.; Gao, L.; He, S. Tunable negative refraction and subwavelength imaging in the metal-dielectric composites of non-spherical particles. *International Symposium on Biophotonics Nano-photonics and Metamaterials* **2006**, 463−466.
(18) Johnson, F. M.; Nethercot, A. H. Antiferromagnetic resonance in MnF_2. *Phys. Rev.* **1959**, *114*, 705−716.
(19) Bloor, D.; Martin, D. H. Antiferromagnetic resonance in the extreme infra-red. *Proc. Phys. Soc., London* **1961**, *78*, 774.
(20) Remer, L.; Lüthi, B.; Sauer, H.; Geick, R.; Camley, R. E. Nonreciprocal optical reflection of the uniaxial antiferromagnet MnF_2. *Phys. Rev. Lett.* **1986**, *56*, 2752−2754.
(21) Almeida, N. S.; Mills, D. L. Dynamical response of antiferromagnets in an oblique magnetic field: Application to surface magnons. *Phys. Rev. B: Condens. Matter Mater. Phys.* **1988**, *37*, 3400−3408.
(22) Nogués, J.; Schuller, I. K. Exchange bias. *J. Magn. Magn. Mater.* **1999**, *192*, 203−232.
(23) Fert, A. Nobel lecture: Origin, development, and future of spintronics*. *Rev. Mod. Phys.* **2008**, *80*, 1517−1530.
(24) Camley, R. E. Nonreciprocal surface waves. *Surf. Sci. Rep.* **1987**, *7*, 103−188.
(25) Kittel, C. Theory of antiferromagnetic resonance. *Phys. Rev.* **1951**, *82*, 565−565.
(26) Nagamiya, T. Theory of antiferromagnetism and antiferromagnetic resonance absorption, ii. *Prog. Theor. Phys.* **1951**, *6*, 350−355.
(27) Mills, D. L.; Burstein, E. Polaritons: the electromagnetic modes of media. *Rep. Prog. Phys.* **1974**, *37*, 817−926.
(28) Boardman, A. D.; Egan, P.; McCall, M. Advanced Metamaterials in Microwaves, Optics and Mechanics. *EPJ. Applied Metamaterials* **2015**, *2*, 11.
(29) Macêdo, R.; Dumelow, T. Tunable all-angle negative refraction using antiferromagnets. *Phys. Rev. B: Condens. Matter Mater. Phys.* **2014**, *89*, 035135.
(30) Bénédicto, J.; Centeno, E.; Moreau, A. Lens equation for flat lenses made with hyperbolic metamaterials. *Opt. Lett.* **2012**, *37*, 4786−4788.
(31) Nye, J. F. *Natural Focusing and Fine Structure of Light: Caustics and Wave Dislocations*; Institute of Physics Publishing: Bristol and Philadelphia, 1999.
(32) Caldwell, J. D.; Kretinin, A. V.; Chen, Y.; Giannini, V.; Fogler, M. M.; Francescato, Y.; Ellis, C. T.; Tischler, J. G.; Woods, C. R.; Giles, A. J.; Hong, M.; Watanabe, K.; Taniguchi, T.; Maier, S. A.; Novoselov, K. S. Sub-difractional volume-confined polaritons in the natural hyperbolic material hexagonal boron nitride. *Nat. Commun.* **2014**, *5*, 5221.
(33) Higuchi, T.; Kanda, N.; Tamaru, H.; Kuwata-Gonokami, M. Selection rules for light-induced magnetization of a crystal with threefold symmetry: The case of antiferromagnetic NiO. *Phys. Rev. Lett.* **2011**, *106*, 047401.
(34) Lan, C.; Bi, K.; Zhou, J.; Li, B. Experimental demonstration of hyperbolic property in conventional material-ferrite. *Appl. Phys. Lett.* **2015**, *107*, 211112.
(35) Macêdo, R.; Stamps, R. L.; Dumelow, T. Spin canting induced nonreciprocal Goos-Hänchen shifts. *Opt. Express* **2014**, *22*, 28467.
(36) Kong, J. A.; Wu, B.-I.; Zhang, Y. Lateral displacement of a gaussian beam reflected from a grounded slab with negative permittivity and permeabilty. *Appl. Phys. Lett.* **2002**, *80*, 2084−2086.
(37) Macêdo, R.; Rodrigues da Silva, R.; Dumelow, T.; da Costa, J. A. P. MgF_2 as a material exhibiting all-angle negative refraction and subwavelength imaging due to the phonon response in the far infrared. *Opt. Commun.* **2014**, *310*, 94−99.
(38) Dumelow, T.; Camley, R. E. Nonreciprocal reflection of infrared radiation from structures with antiferromagnets and dielectrics. *Phys. Rev. B: Condens. Matter Mater. Phys.* **1996**, *54*, 12232−12237.

DOI: 10.1021/acsphotonics.6b00321
ACS Photonics 2016, 3, 1670−1677